Critical divergence of the symmetric (A_{1g}) nonlinear elastoresistance near the nematic transition in an iron-based superconductor

J. C. Palmstrom,[1,2] A. T. Hristov,[2,3] S. A. Kivelson,[2,3] J.-H. Chu,[4] and I. R. Fisher[1,2]

[1]*Geballe Laboratory for Advanced Materials and Department of Applied Physics, Stanford University, Stanford, California 94305, USA*

[2]*Stanford Institute for Materials and Energy Science, SLAC National Accelerator Laboratory, 2575 Sand Hill Road, Menlo Park, California 94025, USA*

[3]*Geballe Laboratory for Advanced Materials and Department of Physics, Stanford University, Stanford, California 94305, USA*

[4]*Department of Physics, University of Washington, Seattle, Washington 98195, USA*

(Received 16 August 2017; published 17 November 2017)

We report the observation of a nonlinear elastoresistivity response for the prototypical underdoped iron pnictide $Ba(Fe_{0.975}Co_{0.025})_2As_2$. Our measurements reveal a large quadratic term in the isotropic (A_{1g}) electronic response that was produced by a purely shear (B_{2g}) strain. The divergence of this quantity upon cooling towards the structural phase transition reflects the temperature dependence of the nematic susceptibility. This observation shows that nematic fluctuations play a significant role in determining even the isotropic properties of this family of compounds.

DOI: 10.1103/PhysRevB.96.205133

I. INTRODUCTION

Nonlinear responses of crystalline materials are described by high rank tensors and can therefore provide valuable information concerning subtle phase transitions and broken symmetries. For example, previous nonlinear measurements of tensor properties have revealed interesting transitions in several strongly correlated materials [1–3]. Here we demonstrate a type of nonlinear transport response associated with changes in the conductivity of a material in response to strain: nonlinear elastoresistivity. This technique allows us to not only look at broken symmetries across a phase transition, but to characterize properties of the disordered state. We perform these measurements for a representative underdoped Fe-based superconductor $Ba(Fe_{0.975}Co_{0.025})_2As_2$, which has previously been shown to exhibit a large nematic susceptibility for temperatures above a tetragonal-to-orthorhombic structural phase transition [4–12]. The most remarkable aspect of the current data is that they reveal a diverging nonlinear response in the *isotropic* elastoresistivity in response to a perfectly *antisymmetric* (shear) strain. This observation, which is intimately tied to the large nematic susceptibility of the material studied, serves to underscore the role played by nematic fluctuations in determining even the isotropic properties of the Fe-based superconductors.

Elastoresistivity relates changes in the resistivity [$\Delta\rho = \rho(\epsilon) - \rho(\epsilon = 0)$] [13] to strains ($\epsilon$) experienced by a material:

$$\left(\frac{\Delta\rho}{\rho_0}\right)_\alpha = \sum_{\bar{\alpha},\bar{\alpha}',\ldots} (m_\alpha^{\bar{\alpha}}\,\epsilon_{\bar{\alpha}} + m_\alpha^{\bar{\alpha}\bar{\alpha}'}\,\epsilon_{\bar{\alpha}}\,\epsilon_{\bar{\alpha}'} + \cdots), \qquad (1)$$

where the α's represent a complete, orthogonal basis set for the system, ϵ_α is the component of the overall strain along a given basis vector, and ρ_0 is an appropriate normalization factor [14]; here the in-plane resistivity of the tetragonal phase. A natural basis to work in is the irreducible representations of the crystallographic point group. In the absence of a magnetic field and in the D_{4h} point group (appropriate for the material studied here), both strain and $\Delta\rho/\rho_0$ have six independent components. Of these, four unique combinations correspond to distinct representations: $(\Delta\rho/\rho_0)_{B_{1g}} = \frac{1}{2}[(\Delta\rho/\rho_0)_{xx} - (\Delta\rho/\rho_0)_{yy}]$, $(\Delta\rho/\rho_0)_{B_{2g}} = (\Delta\rho/\rho_0)_{xy}$, and $(\Delta\rho/\rho_0)_{E_g} = [(\Delta\rho/\rho_0)_{xz},(\Delta\rho/\rho_0)_{yz}]$. Objects with B_{1g} and B_{2g} symmetry are antisymmetric (odd) with respect to a 90° rotation about the z axis. There is also a two-dimensional space of components belonging to the A_{1g} representation, the basis of which is not uniquely defined by symmetry alone [15]. Objects with A_{1g} symmetry are symmetric (even) with respect to a 90° rotation around the z axis. In this paper we focus on one (of the two) components with A_{1g} symmetry reflecting the in-plane changes in resistivity, i.e., $(\Delta\rho/\rho_0)_{A_{1g}} = \frac{1}{2}[(\Delta\rho/\rho_0)_{xx} + (\Delta\rho/\rho_0)_{yy}]$.

The linear elastoresistivity response is described by a fourth rank tensor, which in the present basis corresponds to $m_\alpha^{\bar{\alpha}}$. As shown previously, $m_{B_{1g}}^{B_{1g}}$ and $m_{B_{2g}}^{B_{2g}}$ [16] are proportional to the nematic susceptibility in the corresponding symmetry channels $\chi_{B_{1g}}$ and $\chi_{B_{2g}}$ [4,10–12,14]. To linear order, correctly decomposed symmetry channels cannot mix. For example, for a tetragonal material, antisymmetric strain ($\epsilon_{B_{1g}}$ and $\epsilon_{B_{2g}}$) cannot cause a symmetric resistivity response, i.e., $m_{A_{1g}}^{B_{1g}} = m_{A_{1g}}^{B_{2g}} = 0$. However, this is not true when considering the nonlinear response. In the present work, we demonstrate the presence of a large and strongly temperature dependent nonlinear A_{1g} elastoresistivity in response to antisymmetric B_{2g} strain (i.e., we show that $m_{A_{1g}}^{B_{2g},B_{2g}} \gg 1$). We further show that this behavior reflects the diverging nematic susceptibility of the material.

II. EXPERIMENTAL METHODS

Measuring the elastoresistance in the A_{1g} symmetry channel presents several technical challenges. In order to precisely decompose the elastoresistance response into the isotropic and antisymmetric components, the resistivity in two orthogonal directions must be measured simultaneously *for identical strain conditions*; otherwise, the B_{2g} elastoresistance (which for these materials is much larger than the A_{1g} elastoresistivity response) gets admixed. A second important consideration is that to confidently extract the linear and quadratic A_{1g} elastoresistance coefficients, the sample must be close to

conditions of neutral anisotropic strain ($\epsilon_{x'x'} - \epsilon_{y'y'} \approx 0$; here the primed coordinate frame refers to the normal strain frame [14]). As we demonstrate, a modified Montgomery technique is especially suitable for both purposes [4]. The crystals are cut into thin square plates with the electrical contacts made at the four corners, enabling measurement of $\rho_{x'x'}$ and $\rho_{y'y'}$ simultaneously, while the crystal is held under a measured set of strain conditions. The B_{2g} neutral strain point is determined by the condition of $\rho_{x'x'} = \rho_{y'y'}$, since for a crystal with tetragonal symmetry the in-plane resistivity is isotropic if there is zero anisotropic strain.

In our experimental setup, we apply biaxial stress to the samples by affixing them to a lead-zirconate-titanate (PZT) stack (Part No.: PSt150/5x5/7 cryo 1, from Piezomechanik GmbH). When positive voltage is applied to the PZT stack, it expands along its poling axis (the y' axis) and contracts along the perpendicular axis (the x' axis). For thin samples, the crystal deforms with the PZT stack. The ratio of the strain experienced by the sample along the y' and x' axes is dictated by the in-plane Poisson ratio ν_P of the PZT stack ($\epsilon_{y'y'} = -\nu_P \epsilon_{x'x'}$). This is a weakly temperature dependent quantity, with an average value for our PZT stacks of ~2.3. Since the magnitude of strains along the x' and y' directions are not equal, the strain can be decomposed into two parts: a part that is even with respect to rotation by 90° about the z axis [in-plane A_{1g} symmetry; $\epsilon_{A_{1g}} = \frac{1}{2}(\epsilon_{x'x'} + \epsilon_{y'y'})$], and an odd part [$B_{1g/2g}$ symmetry; $\epsilon_{B_{1g/2g}} = \frac{1}{2}(\epsilon_{x'x'} - \epsilon_{y'y'})$]. As shown in the inset of Fig. 1, by aligning the sample's square edges along either the tetragonal [100] or tetragonal [110] direction, we selectively cause the material to experience $A_{1g} + B_{1g}$ symmetry strain (pink) or $A_{1g} + B_{2g}$ symmetry strain (blue). Further details about the sample preparation, experimental protocol, and characterization of the strain transmission can be found in Appendices A and B.

III. RESULTS AND DISCUSSION

There is a qualitative difference in the strain dependence of the elastoresistivity between samples that experience B_{1g} and B_{2g} symmetry strain. Figure 1 shows representative data for $Ba(Fe_{0.975}Co_{0.025})_2As_2$ above the structural phase transition. Multiple samples of both orientations have been measured and are in good agreement with the representative data shown here. The sample that experiences B_{1g} strain exhibits a linear change in $\rho_{x'x'}$ and $\rho_{y'y'}$ under strain. Consequently, both the antisymmetric response $[(\Delta\rho/\rho_0)_{B_{1g}}]$ and the symmetric response $[(\Delta\rho/\rho_0)_{A_{1g}}]$ are also linear in strain. In contrast, the sample that experiences B_{2g} strain exhibits a clear nonlinearity in both $\rho_{x'x'}$ and $\rho_{y'y'}$ as the strain is varied. The antisymmetric (B_{2g}) response is perfectly linear [black line in Fig. 1(b)(ii)] and comparatively large, whereas the symmetric (A_{1g}) response exhibits a striking nonlinearity and is well fit by a quadratic function [black line in Fig. 1(b)(iii)]. The minimum of the quadratic function does not occur at the same strain as the neutral B_{2g} strain point [vertical line in Fig. 1(b)], indicating the presence of a linear term in addition to the quadratic coefficient.

The qualitative behavior shown in Fig. 1 is characteristic of both crystal orientations for the range of measured temperatures. Data of the elastoresistance response at different

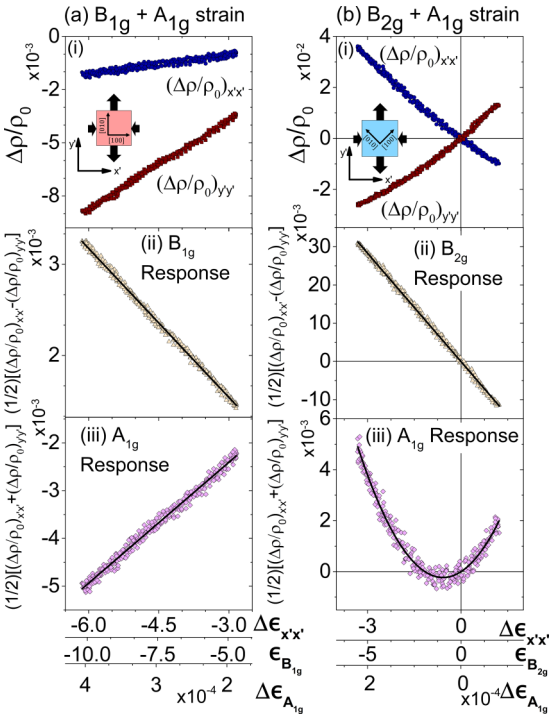

FIG. 1. Representative data showing the resistivity response to strain of $Ba(Fe_{0.975}Co_{0.025})_2As_2$ at 116 K. The left-hand column (a) shows data for a crystal oriented with the crystal axes parallel to the normal strain frame [represented by the schematic pink-colored crystal in the inset to (a)(i)], such that the crystal experiences an admixture of A_{1g} and B_{1g} symmetry strain. The right-hand column (b) shows data for a crystal with the axes oriented at 45 deg to the normal strain frame [shown schematically by the blue crystal in the inset to (b)(i)], such that the crystal experiences an admixture of A_{1g} and B_{2g} symmetry strain. The top graph (i) in each column shows the resistive response of the sample along the x' and y' axes due to the strain, where the x' and y' axes are defined by the normal strain frame (inset). The zero antisymmetric strain condition is marked by a vertical line in (b). The middle graph (ii) shows the antisymmetric response, given by the difference $\frac{1}{2}[(\Delta\rho/\rho_0)_{x'x'} - (\Delta\rho/\rho_0)_{y'y'}] = (\frac{\Delta\rho}{\rho_0})_{B_{1g}/B_{2g}}$. For both crystal orientations, the antisymmetric response is linear (black lines show linear fits). The bottom graph (iii) shows the symmetric (A_{1g}) response, given by the sum $\frac{1}{2}[(\Delta\rho/\rho_0)_{x'x'} + (\Delta\rho/\rho_0)_{y'y'}] = (\frac{\Delta\rho}{\rho_0})_{A_{1g}}$. This response is found to be always linear for samples that experience $A_{1g} + B_{1g}$ symmetry strain (black line shows linear fit), while that of the samples that experience $A_{1g} + B_{2g}$ symmetry strain is clearly nonlinear and is fit by a second order polynomial (black line).

temperatures are shown in Fig. 2 for the sample that was oriented to experience B_{2g} symmetry strain. For this crystal orientation, the antisymmetric response is linear for all temperatures measured, with a slope that grows larger as temperature decreases. Similarly, the symmetric (A_{1g}) response exhibits a strong temperature dependence, with a clear increase in the coefficient of the quadratic term as temperature is reduced towards the structural transition. In contrast, the sample that experiences B_{1g} symmetry strain exhibits only a weak temperature dependence in the linear response for both symmetry channels, as shown in Fig. 1(a), and never exhibits any measurable nonlinearity.

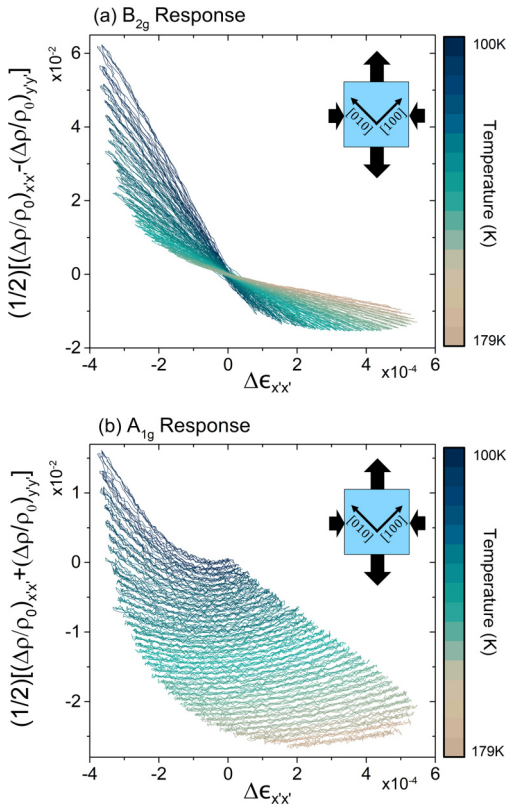

FIG. 2. Temperature dependence of (a) the antisymmetric (B_{2g}) elastoresistivity response, and (b) the isotropic (A_{1g}) elastoresistivity response, of a single crystal of $Ba(Fe_{0.975}Co_{0.025})_2As_2$ oriented with the crystal axes at 45 deg to the normal strain frame (blue schematic insets). The anisotropic response is always linear, whereas the isotropic response shows a large quadratic component with a minimum close to the B_{2g} neutral strain point. Both responses exhibit a strong temperature dependence. Note that the accessible strain range shifts with temperature, due in part to differences in the thermal expansion of the PZT and sample, and in part to the temperature dependence of the dynamic range of the PZT stack. For clarity, each fixed temperature strain sweep for the A_{1g} response are offset by -7.5×10^{-4} per trace from the 100 K sweep. The data showing the B_{2g} response are not offset.

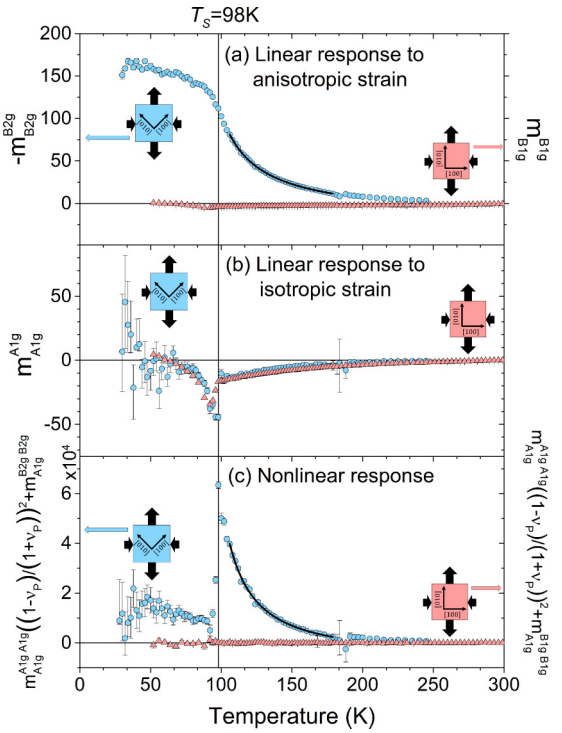

FIG. 3. Temperature dependence of the elastoresistance coefficients of $Ba(Fe_{0.975}Co_{0.025})_2As_2$ for all symmetry channels measured. Blue circles show the response for a sample that experiences an admixture of $A_{1g} + B_{2g}$ symmetry strain (blue schematic insets), while pink triangles show the response for a sample that experiences an admixture of $A_{1g} + B_{1g}$ symmetry strain (pink schematic insets). (a) The linear response to anisotropic strain, $m_{B_{2g}}^{B_{2g}}$ (left axis) and $m_{B_{1g}}^{B_{1g}}$ (right axis). $m_{B_{2g}}^{B_{2g}}$ can be well fit by a Curie-Weiss functional form (black line; see main text). (b) The linear response to isotropic strain $m_{A_{1g}}^{A_{1g}}$. For crystals that experience $A_{1g} + B_{1g}$ symmetry strain (pink), $m_{A_{1g}}^{A_{1g}}$ is extracted from a linear fit; for crystals that experience $A_{1g} + B_{2g}$ symmetry strain (blue), the data are extracted from the linear term of a second order polynomial fit. (c) The weighted quadratic coefficients $[(\frac{1-\nu_P}{1+\nu_P})^2 m_{A_{1g}}^{A_{1g},A_{1g}} + m_{A_{1g}}^{B_{2g},B_{2g}}]$ (blue data, left axis) and $[(\frac{1-\nu_P}{1+\nu_P})^2 m_{A_{1g}}^{A_{1g},A_{1g}} + m_{A_{1g}}^{B_{1g},B_{1g}}]$ (pink data, right axis) describing the isotropic response to $(A_{1g} + B_{2g})$ and $(A_{1g} + B_{1g})$ symmetry strains, respectively, extracted from the second order polynomial fit of the isotropic response as a function of anisotropic strain. The only measurably nonzero nonlinear coefficient is $m_{A_{1g}}^{B_{2g},B_{2g}}$, the isotropic response to B_{2g} symmetry anisotropic strain. The temperature-dependence of this coefficient can be well fit by $\frac{a}{(T-\Theta)^2} + \frac{b}{T-\Theta} + c$ (black line; see main text), with Θ taken from the Curie-Weiss fit to $m_{B_{2g}}^{B_{2g}}$. Error bars represent 95% confidence intervals from statistical fits. If an error bar is not shown, the uncertainty of the fit is contained within the size of the data point.

We first consider the linear response to antisymmetric strains $m_{B_{1g}}^{B_{1g}}$ and $m_{B_{2g}}^{B_{2g}}$ shown in Fig. 3(a). As found previously [12], $m_{B_{1g}}^{B_{1g}}$ is small and exhibits almost no temperature dependence. In contrast, $m_{B_{2g}}^{B_{2g}}$ is large and can be well fit by a Curie-Weiss temperature dependence with a Weiss temperature $\Theta = 75.8 \pm 0.6$ K (adjusted R-squared, $R^2_{\text{adj}} = 0.9995$), bearing witness to the divergent nematic susceptibility in this material [4,10–12]. The coupled nematic/structural phase transition occurs at a higher temperature $T_s = 98 \pm 2$ K due to bilinear coupling between the nematic order parameter and lattice strain with the same symmetry [10].

The linear response to A_{1g} strain $m_{A_{1g}}^{A_{1g}}$ is small and only weakly temperature dependent [Fig. 3(b)] [17]. Moreover, values of $m_{A_{1g}}^{A_{1g}}$ determined from both crystal orientations agree [as they must, since by symmetry both $\epsilon_{A_{1g}}$ and $(\Delta\rho/\rho_0)_{A_{1g}}$ are invariant to rotations about the z axis], providing additional confidence that the B_{2g} neutral strain point has been accurately identified. For further discussion of errors associated with identification of the neutral strain point, see Appendix C.

From a symmetry perspective, nonlinear contributions to $(\Delta\rho/\rho_0)_{A_{1g}}$ are possible due to all three strains considered.

To quadratic order,

$$\left(\frac{\Delta\rho}{\rho_0}\right)_{A_{1g}} = m_{A_{1g}}^{A_{1g}}\,\epsilon_{A_{1g}} + m_{A_{1g}}^{A_{1g},A_{1g}}\,[\epsilon_{A_{1g}}]^2 + m_{A_{1g}}^{B_{1g},B_{1g}}\,[\epsilon_{B_{1g}}]^2 + m_{A_{1g}}^{B_{2g},B_{2g}}\,[\epsilon_{B_{2g}}]^2. \quad (2)$$

Since the symmetric and antisymmetric strains are related via ν_P (i.e., $\epsilon_{B_{1g/2g}} = \frac{(1+\nu_P)}{(1-\nu_P)}\epsilon_{A_{1g}}$), the quadratic coefficient of $(\Delta\rho/\rho_0)_{A_{1g}}$ as a function of $\epsilon_{B_{1g/2g}}$ is given by the weighted sum of coefficients $m_{A_{1g}}^{B_{1g},B_{1g}/B_{2g},B_{2g}} + (\frac{1-\nu_P}{1+\nu_P})^2 m_{A_{1g}}^{A_{1g},A_{1g}}$ for $A_{1g} + B_{1g/2g}$ symmetry strains, respectively. The temperature dependence of these weighted sums, obtained from quadratic fits to the data shown in Fig. 2(b) with appropriate transformation of the strain axis, are plotted in Fig. 3(c). Evidently, $m_{A_{1g}}^{A_{1g},A_{1g}}$ and $m_{A_{1g}}^{B_{1g},B_{1g}}$ (the weighted sum of which is shown by the pink data) are vanishingly small. Hence, the striking nonlinear response seen in Fig. 2(b) derives solely from $m_{A_{1g}}^{B_{2g},B_{2g}}$, that is, *the nonlinear symmetric response derives solely from purely antisymmetric (B_{2g}) strain*.

The Curie-Weiss temperature dependence of $m_{B_{2g}}^{B_{2g}}$ directly attests to the presence of an electronic degree of freedom (the nematic order parameter $\phi_{B_{2g}}$) that is separate from, though bi-linearly coupled to, anisotropic strain $\epsilon_{B_{2g}}$: $\phi_{B_{2g}} = \chi_{B_{2g}}\epsilon_{B_{2g}} \propto m_{B_{2g}}^{B_{2g}}\epsilon_{B_{2g}}$. From the same perspective, in addition to a bare contribution to $(\Delta\rho/\rho_0)_{A_{1g}}$ that is directly proportional to $[\epsilon_{B_{2g}}]^2$, there should be additional induced terms proportional to $\phi_{B_{2g}}\epsilon_{B_{2g}}$ and $[\phi_{B_{2g}}]^2$. All these terms are allowed by symmetry, and since $\phi_{B_{2g}} = \chi_{B_{2g}}\epsilon_{B_{2g}}$, the latter two contributions should be increasingly strong with decreasing temperature, so that

$$m_{A_{1g}}^{B_{2g},B_{2g}} \approx \frac{a}{(T-\Theta)^2} + \frac{b}{T-\Theta} + c, \quad (3)$$

where a, b, and c are coefficients to be determined. The Weiss temperature Θ, which is independently determined from the temperature dependence of $m_{B_{2g}}^{B_{2g}}$, is not a fit parameter. The black line in Fig. 3(c) shows the best fit to this functional form, with $\sqrt{a} = (4 \pm 1) \times 10^3$ K and $b = (7 \pm 1) \times 10^5$ K; both terms are important and necessary to fully fit the response (see Appendix D for more details on the fitting). This fit is in excellent agreement with the data ($R^2_{\text{adj}} = 0.99655$) and confirms our understanding of the contributing symmetry terms and the underlying physics. The quality of fit also implies that the proportionality constant relating $\chi_{B_{2g}}$ and the elastoresistivity coefficients have negligible temperature dependence over the fit range.

Finally, we note that $m_{A_{1g}}^{B_{2g},B_{2g}}$ is positive. This implies that the average resistance is expected to be larger in the anisotropic nematic phase than an extrapolation of the in-plane resistivity determined from the isotropic tetragonal state. Since this is a second order effect, we expect the resistivity increase to scale as the square of the on-setting nematic order parameter, i.e., to have a T-linear temperature dependence, for temperatures close to T_s. This is consistent with the observation [18] that the resistivity of twinned $Ba(Fe_{0.975}Co_{0.025})_2As_2$ samples linearly increases upon cooling through the structural transition [19].

IV. SUMMARY

In summary, we have shown a diverging nonlinear A_{1g} elastoresistivity response to B_{2g} symmetry strain. The most remarkable aspect of this measurement is not that $m_{A_{1g}}^{B_{2g},B_{2g}} \neq 0$, since this is allowed by symmetry, but how large this quantity is. Indeed, close to the structural transition the nonlinear response of $(\Delta\rho/\rho_0)_{A_{1g}}$ to $\epsilon_{B_{2g}}$ is an order of magnitude larger than the linear response to $\epsilon_{A_{1g}}$ for the range of strain considered here. Furthermore, the temperature dependence of this coefficient directly reveals that the effect is driven by the large nematic susceptibility of the material, meaning that even the isotropic properties of the Fe-based superconductors [in this case $(\Delta\rho/\rho_0)_{A_{1g}}$] are strongly affected by the nematic character of the material. These observations demonstrate a means to witness the divergent nematic susceptibility in these materials based on the measurement of the *isotropic* response to anisotropic strain. They also provide a point of comparison for microscopic models of the transport properties of Fe-based superconductors.

ACKNOWLEDGMENTS

J.C.P. and A.T.H. are supported by a NSF Graduate Research Fellowship (Grant No. DGE-114747). J.C.P. is also supported by a Gabilan Stanford Graduate Fellowship. J.-H.C. acknowledges the support from the State of Washington funded Clean Energy Institute. This work was supported by the Department of Energy, Office of Basic Energy Sciences, under Contract No. DE-AC02-76SF00515.

APPENDIX A: FURTHER DETAILS OF SAMPLE PREPARATION AND EXPERIMENTAL PROTOCOL

Single crystals of $Ba(Fe_{0.975}Co_{0.025})_2As_2$ were grown using the FeAs self-flux technique as described elsewhere [18]. The crystals were cleaved into thin plates and cut into approximately square rectilinear tablets with typical side lengths of 400–750 μm and thicknesses of 10–30 μm. The B_{2g} sample shown in the main text has dimensions 30 μm × 730 μm × 700 μm and the B_{1g} sample has dimensions 10 μm × 540 μm × 530 μm. The modified Montgomery method assumes square isotropic equivalent samples, however deviations from square, up to roughly side length ratios of 4:1, introduce errors significantly smaller than the errors from Taylor series truncations (∼4%) used in the method [20]. The roughly square geometry does ensure equal strain relaxation in both the x' and y' directions. The samples are contacted on the corners of their top surface by gold wires affixed with an air-dry silver epoxy (Dupont 4929N) on sputtered gold pads. The samples are glued to a PZT stack (Part No.: PSt150/5x5/7 cryo 1, from Piezomechanik GmbH) with either Devcon 5-min epoxy or Master Bond EP21TCHT-1. A photograph of a typical sample and a diagram of the PZT setup can be seen in Fig. 4. Stress was applied to the sample by stepwise cycling the voltage from −150 to 150 V (below 150 K) and −50 to 150 V (above 150 K) on the PZT stack at a fixed temperature. Three to four voltage sweeps were performed at each temperature,

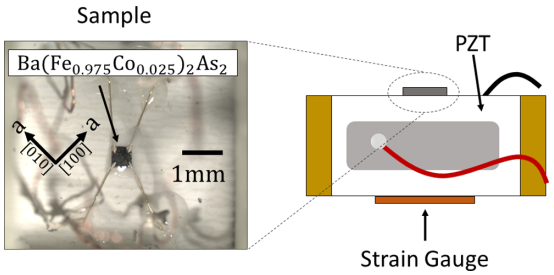

FIG. 4. Left: Photograph of a representative $Ba(Fe_{0.975}Co_{0.025})_2As_2$ sample prepared for an elastoresistance measurement using the modified Montgomery method. The sample is cut into a square, affixed with electrical contacts, and glued onto the PZT stack. This sample is aligned with its crystallographic axes rotated 45 deg with respect to the normal strain frame. Right: Schematic diagram showing the PZT stack prepared for an elastoresistance measurement, seen from the side. The sample is glued to the top face of the PZT. Strain is measured via a strain gauge glued to the back of the PZT stack.

with typical voltage ramp rates between 8–15 V/s. Using the modified Montgomery method [4,20], $\rho_{x'x'}$ and $\rho_{y'y'}$ were measured simultaneously at each voltage step.

The strain of the PZT stack is measured by a strain gauge (Part No.: WK-06-062TT-350 from VPG) glued to the back of the PZT stack. Typically only one direction of strain is measured and the orthogonal strain is calculated using the measured Poisson ratio of the PZT stack ($\epsilon_{y'y'} = -\nu_P \epsilon_{x'x'}$) [12]. For measurements done here we assume perfect strain transmission through the glue and sample such that the strain experienced by the sample is the same as the strain of the PZT stack. Imperfect strain transmission would scale the resistive response in all symmetry channels, but would neither change our symmetry decomposition nor affect our main conclusions. This is discussed in detail in Appendix B.

Both the glue and the PZT stack have differing coefficients of thermal expansion, neither of which are matched to the pnictide sample. In addition, the glue will contract as it dries during the mounting of the sample which can introduce uncontrolled strains. All of these factors contribute to a temperature dependence of the voltage required to have the sample experience zero antisymmetric strain. There does not appear to be a common trend between samples in the evolution of this neutral point as a function of temperature. For example, the evolution is often nonmonotonic and net changes are evenly split between shifts to positive voltages and negative voltages among the six samples measured. This indicates that this effect is not solely due to differential thermal contractions of the sample on PZT, implying that the epoxy plays a significant role in determine the bias strain experienced by the sample when zero volts are applied to the PZT stack.

APPENDIX B: STRAIN TRANSMISSION

The strain transmission through the crystal will depend on geometric factors; for example, the thicker the crystal is compared with the in-plane dimensions, the more the strain will relax along the z axis of the crystal. In order to quantify

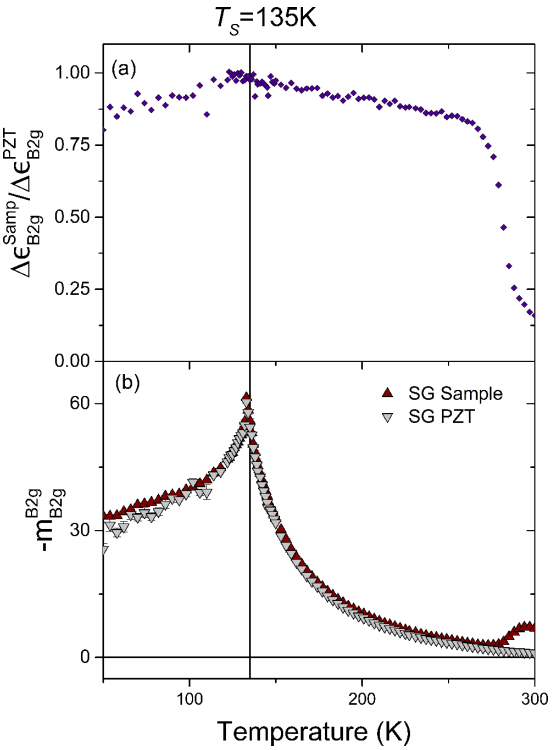

FIG. 5. Strain transmission through a large (3140 μm $\times$ 3330 μm $\times$ 50 μm) $BaFe_2As_2$ crystal under $A_{1g} + B_{2g}$ symmetry strains. A strain gauge is glued on top of the sample ($\Delta\epsilon^{\text{Samp}}_{y'y'}$) and a second strain gauge is affixed directly to the back of the PZT stack ($\Delta\epsilon^{\text{PZT}}_{y'y'}$). For this particular test, $\Delta\epsilon_{x'x'}$ is estimated based on the measured Poisson ratio of the PZT, allowing for the estimation of the antisymmetric strains $\Delta\epsilon^{\text{PZT}}_{B_{2g}}$ and $\Delta\epsilon^{\text{Samp}}_{B_{2g}}$; $\frac{1}{2}(\Delta\epsilon^{\text{PZT}}_{x'x'} - \Delta\epsilon^{\text{PZT}}_{y'y'})$ and $\frac{1}{2}(\Delta\epsilon^{\text{Samp}}_{x'x'} - \Delta\epsilon^{\text{Samp}}_{y'y'})$, respectively. (a) The temperature dependence of the ratio of the range of antisymmetric strain experienced by the two strain gauges during fixed temperature voltage sweeps. Below 250 K the strain transmission through the samples is $\geqslant 80\%$ and only has a weak temperature dependence. (b) The extracted $m^{B_{2g}}_{B_{2g}}$ elastoresistivity response calculated from both strain gauges. The two traces are in good agreement below 250 K, indicating that the temperature dependence of the response is dominated by the intrinsic temperature dependence of the electronic sample properties over the temperature dependence of the strain transmission.

the strain transmission we compare a strain gauge mounted on top of a large undoped $BaFe_2As_2$ sample prepared as described in Appendix A and a strain gauge glued directly to the back of the PZT stack. For this experiment we measure the range of strain along the y' direction for the sample mounted strain gauge ($\Delta\epsilon^{\text{Samp}}_{y'y'}$) and for the PZT mounted strain gauge ($\Delta\epsilon^{\text{PZT}}_{y'y'}$) for fixed temperature voltage sweeps. The range of strain along the x' direction is estimated based on the Poisson ratio of the PZT stack. From this we can calculate the range of antisymmetric strain experienced by the sample strain gauge [$\Delta\epsilon^{\text{Samp}}_{B_{2g}} = \frac{1}{2}(\Delta\epsilon^{\text{Samp}}_{x'x'} - \Delta\epsilon^{\text{Samp}}_{y'y'})$] and PZT strain gauge [$\Delta\epsilon^{\text{PZT}}_{B_{2g}} = \frac{1}{2}(\Delta\epsilon^{\text{PZT}}_{x'x'} - \Delta\epsilon^{\text{PZT}}_{y'y'})$]. The temperature dependence of the ratio $\Delta\epsilon^{\text{Samp}}_{B_{2g}}/\Delta\epsilon^{\text{PZT}}_{B_{2g}}$ is shown in Fig. 5(a), a ratio of one implies perfect strain transmission through the sample. At 270 K there is a sharp increase in strain transmission

which we attribute to a freezing transition of the glue. Below 250 K the strain transmission is $\geqslant 80\%$ and has only a weak temperature dependence. This temperature dependence is small compared with the temperature dependence of the elastoresistance response which is demonstrated in Fig. 5(b) where $m_{B_{2g}}^{B_{2g}}$ is calculated twice, once using the measured strain of the strain gauge mounted on the sample and once using the measured strain of the strain gauge mounted on the PZT stack. The two calculations are in good agreement below 250 K.

The majority of samples are too small to accommodate a strain gauge on their surface. To quantify the strain transmission as a function of sample size, three undoped $BaFe_2As_2$ samples: small (280 μm × 300 μm × 20 μm), medium (760 μm × 750 μm × 40 μm), and large (3140 μm × 3330 μm × 50 μm, this sample is large enough to have a strain gauge on its surface and is the sample measured for the data shown in Fig. 5) were measured. The extracted $m_{B_{2g}}^{B_{2g}}$ responses are shown in Fig. 6(a). In these calculations of $m_{B_{2g}}^{B_{2g}}$, strain was measured by a strain gauge glued to the back of the PZT stack and the strain was assumed to be fully transmitted, i.e., the sample experiences the same strain as the PZT stack. The large and medium samples have the same temperature dependence and magnitude of response, indicating that both samples have similar strain transmission ($\geqslant 80\%$). While the magnitude of the response of the small sample is significantly reduced, likely due to an overestimation of the strain experienced by the sample. This implies that for the small sample either the crystal is positioned on the PZT stack such that it experiences a smaller strain or that there is a strain gradient along the z crystallographic axis and that the sample experiences an E_g shear strain ($\epsilon_{x'z'}$,$\epsilon_{y'z'}$). By normalizing the $m_{B_{2g}}^{B_{2g}}$ response at the structural transition $T_S = 135$ K, the temperature dependence of the small and large samples can be compared. This is shown in Fig. 6(b). The two normalized responses are in good agreement below 250 K, which demonstrates that imperfect strain transmission results in only a simple scaling of the magnitude of the elastoresistance response.

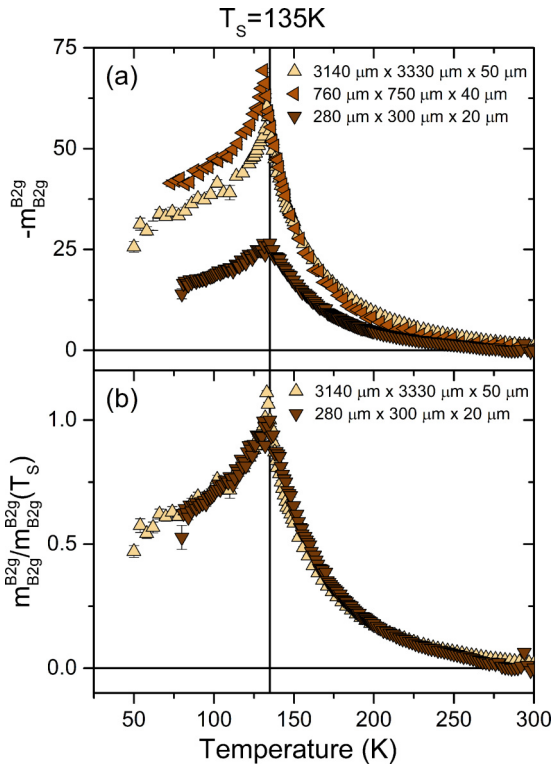

FIG. 6. Comparison of sample size on the linear anisotropic elastoresistivity response $m_{B_{2g}}^{B_{2g}}$ and strain transmission in $BaFe_2As_2$. Three sample sizes are studied: small (280 μm × 300 μm × 20 μm), medium (3760 μm × 750 μm × 40 μm), and large (3140 μm × 3330 μm × 50 μm). The strain at the surface of the large sample has been measured to be $\geqslant 80\%$ below 250 K (Fig. 5). For the data shown here the strain is measured by a strain gauge glued directly to the PZT stack and strain is assumed to be fully transmitted from the PZT to the sample. The top plot (a) shows $m_{B_{2g}}^{B_{2g}}$ data for all three samples. The elastoresistivity responses of the medium and large samples have the same magnitude and temperature dependence suggesting they are in a regime of similar strain transmission ($\geqslant 80\%$). The small sample has a significantly smaller response. This is attributed to imperfect strain transmission in the smallest sample, resulting in the overestimation of the strain experienced by the sample. The bottom plot (b) shows the normalized elastoresistivity response for the small and large sample. The two curves exhibit the same temperature dependence, indicating that imperfect strain transmission results in a temperature independent scaling of the response.

This allows us to use the magnitude of the $m_{B_{2g}}^{B_{2g}}$ response as an approximate measure of strain transmission, with the assumption that samples with in-plane dimensions ~750 μm or larger have $\geqslant 80\%$ strain transmission. For samples oriented to experience B_{1g} strain estimating the overall strain transmission is more challenging. Rough estimates can be made based off of their relative size compared to samples that experience B_{2g} strain. The B_{2g} sample shown in the main text (30 μm × 730 μm × 700 μm) has $\geqslant 80\%$ strain transmission, while the B_{1g} sample (10 μm × 540 μm × 530 μm) has $\geqslant$60%–80% strain transmission.

APPENDIX C: ERRORS IN EXTRACTING THE LINEAR AND QUADRATIC RESPONSE FROM $\rho_{A_{1g}}$ ARISING FROM UNCERTAINTY IN IDENTIFYING THE NEUTRAL STRAIN POINT

As shown in the main text, the main finding of the current work is that for the strain ranges we employ the elastoresistance of $Ba(Fe_{0.975}Co_{0.025})_2As_2$ is linear with the exception of a large nonlinear $m_{A_{1g}}^{B_{2g},B_{2g}}$ term. However, due to differences in the thermal expansion of the PZT, sample, and the glue holding the sample in place, and the volume contraction of the glue as it dries when the sample is attached to the PZT stack, the sample once mounted and cooled may experience external strains even when no voltage is applied to the PZT stack. The neutral B_{2g} and A_{1g} strain points may even be offset from each other. Since the PZT applies a fixed ratio of symmetric and antisymmetric strains, if there is an offset in the neutral points at best we can tune through one neutral point at a time (i.e., $\epsilon_{A_{1g}} = 0$ or $\epsilon_{B_{2g}} = 0$).

We can identify the neutral antisymmetric strain point above the tetragonal to orthorhombic structural transition (98 K) because, for a tetragonal material at the neutral antisymmetric strain point, $\rho_{xx} = \rho_{yy}$. The modified Montgomery method is well suited to identify the antisymmetric strain neutral point since it simultaneously measures $\rho_{x'x'}$ and $\rho_{y'y'}$ under identical strain conditions in a single sample. This is one advantage of the modified Montgomery method over the previously used differential technique [12]. It is more challenging to identify the symmetric strain neutral point and it is not done in this work. Below is a detailed calculation of the effects of the misidentification of strain offsets on the calculated elastoresistivity tensor components. For simplicity we look at an offset in $\epsilon_{x'x'}$ which still allows for tuning to the neutral point of both A_{1g} and $B_{1g/2g}$ symmetry strains, but the results hold even if the neutral points are separated. The main conclusions are that, for this material, the correct identification of the antisymmetric neutral point is required to accurately estimate $m^{A_{1g}}_{A_{1g}}$ for samples that experience A_{1g} and B_{2g} symmetry strain, however neither $m^{B_{1g/2g}}_{B_{1g/2g}}$ nor $m^{B_{1g/2g},B_{1g/2g}}_{A_{1g}}$ are dependent on the identification of the neutral point. All results are robust to the determination of the symmetric strain neutral point.

We start with the simple case of the linear antisymmetric response, assuming no offset between the neutral A_{1g} and $B_{1g/2g}$ strain points and that $\epsilon_{A_{1g}}$, $\epsilon_{B_{1g/2g}}$, and $\epsilon_{x'x'}$ are all measured relative to the neutral point where $\epsilon_{A_{1g}} = \epsilon_{B_{1g/2g}} = \epsilon_{x'x'} = 0$. Then the change in antisymmetric resistivity to $\epsilon_{x'x'}$ is described by

$$(\Delta\rho/\rho_0)_{B_{1g/2g}} = m^{B_{1g/2g}}_{B_{1g/2g}}\epsilon_{B_{1g/2g}} = m^{B_{1g/2g}}_{B_{1g/2g}}\left(\frac{1+\nu_P}{2}\right)\epsilon_{x'x'}. \tag{C1}$$

If the neutral strain point is misidentified by an amount $\Delta\epsilon_{x'x'}$, such that $\epsilon^{\text{true}}_{x'x'} = \epsilon^{\text{meas}}_{x'x'} + \Delta\epsilon_{x'x'}$, then there will be an offset in both the symmetric and antisymmetric neutral points (i.e., $\Delta\epsilon_{A_{1g}} = \frac{1-\nu_P}{2}\Delta\epsilon_{x'x'}$ and $\Delta\epsilon_{B_{2g}} = \frac{1+\nu_P}{2}\Delta\epsilon_{x'x'}$). Then the antisymmetric response becomes

$$(\Delta\rho/\rho_0)_{B_{1g/2g}} = m^{B_{1g/2g}}_{B_{1g/2g}}\left(\frac{1+\nu_P}{2}\right)(\epsilon^{\text{meas}}_{x'x'} + \Delta\epsilon_{x'x'}). \tag{C2}$$

The linear antisymmetric elastoresistivity coefficient is extracted from the slope of the linear fit of $(\Delta\rho/\rho_0)_{B_{1g/2g}}$ vs $\frac{1+\nu_P}{2}\epsilon^{\text{meas}}_{x'x'}$ ($\epsilon^{\text{meas}}_{B_{1g/2g}}$). In this case the extracted slope is the true elastoresistivity coefficient $m^{B_{1g/2g}}_{B_{1g/2g}}$, independent of the error in the identification of the strain neutral point $\Delta\epsilon_{x'x'}$.

For the isotropic resistivity response, we again start by assuming no offset between the neutral symmetric and antisymmetric strain points and that all strains are measured relative to the neutral point where $\epsilon_{A_{1g}} = \epsilon_{B_{1g/2g}} = \epsilon_{x'x'} = 0$. For simplicity we will perform these calculations for a sample that experiences A_{1g} and B_{2g} symmetry strain (the same calculation can be done for a sample that experiences A_{1g} and B_{1g} symmetry strains by simply replacing all references to B_{2g} with B_{1g}). The isotropic resistivity response is then described by

$$\begin{aligned}(\Delta\rho/\rho_0)_{A_{1g}} &= m^{A_{1g}}_{A_{1g}}\epsilon_{A_{1g}} + m^{A_{1g},A_{1g}}_{A_{1g}}[\epsilon_{A_{1g}}]^2 + m^{B_{2g},B_{2g}}_{A_{1g}}[\epsilon_{B_{2g}}]^2 \\ &= m^{A_{1g}}_{A_{1g}}\left(\frac{1-\nu_P}{2}\right)\epsilon_{x'x'} + m^{A_{1g},A_{1g}}_{A_{1g}} \\ &\quad\times\left[\left(\frac{1-\nu_P}{2}\right)\epsilon_{x'x'}\right]^2 \\ &\quad + m^{B_{2g},B_{2g}}_{A_{1g}}\left[\left(\frac{1+\nu_P}{2}\right)\epsilon_{x'x'}\right]^2. \end{aligned}\tag{C3}$$

Now we introduce a misidentification of the neutral strain point by an amount $\Delta\epsilon_{x'x'}$ ($\epsilon^{\text{true}}_{x'x'} = \epsilon^{\text{meas}}_{x'x'} + \Delta\epsilon_{x'x'}$). The isotropic resistivity response then becomes

$$\begin{aligned}(\Delta\rho/\rho_0)_{A_{1g}} &= \left[\left(\frac{1-\nu_P}{1+\nu_P}\right)^2 m^{A_{1g},A_{1g}}_{A_{1g}} + m^{B_{2g},B_{2g}}_{A_{1g}}\right] \\ &\quad\times\left[\frac{1+\nu_P}{2}\epsilon^{\text{meas}}_{x'x'}\right]^2 \\ &\quad + \Big[m^{A_{1g}}_{A_{1g}} + m^{A_{1g},A_{1g}}_{A_{1g}}(1-\nu_P)\Delta\epsilon_{x'x'} \\ &\quad + m^{B_{2g},B_{2g}}_{A_{1g}}\frac{(1+\nu_P)^2}{1-\nu_P}\Delta\epsilon_{x'x'}\Big]\frac{1-\nu_P}{2}\epsilon^{\text{meas}}_{x'x'} \\ &\quad + m^{A_{1g}}_{A_{1g}}\frac{1-\nu_P}{2}\Delta\epsilon_{x'x'} \\ &\quad + m^{A_{1g},A_{1g}}_{A_{1g}}\left[\left(\frac{1-\nu_P}{2}\right)\Delta\epsilon_{x'x'}\right]^2 \\ &\quad + m^{B_{2g},B_{2g}}_{A_{1g}}\left[\left(\frac{1+\nu_P}{2}\right)\Delta\epsilon_{x'x'}\right]^2. \end{aligned}\tag{C4}$$

For this material the only non-negligible quadratic response is $m^{B_{2g},B_{2g}}_{A_{1g}}$ ($m^{B_{1g},B_{1g}}_{A_{1g}} \approx m^{A_{1g},A_{1g}}_{A_{1g}} \approx 0$). This further simplifies the equation

$$\begin{aligned}(\Delta\rho/\rho_0)_{A_{1g}} &\approx m^{B_{2g},B_{2g}}_{A_{1g}}\left[\frac{1+\nu_P}{2}\epsilon^{\text{meas}}_{x'x'}\right]^2 \\ &\quad + \left(m^{A_{1g}}_{A_{1g}} + m^{B_{2g},B_{2g}}_{A_{1g}}\frac{(1+\nu_P)^2}{1-\nu_P}\Delta\epsilon_{x'x'}\right) \\ &\quad\times\frac{1-\nu_P}{2}\epsilon^{\text{meas}}_{x'x'} + m^{A_{1g}}_{A_{1g}}\frac{1-\nu_P}{2}\Delta\epsilon_{x'x'} \\ &\quad + m^{B_{2g},B_{2g}}_{A_{1g}}\left[\left(\frac{1+\nu_P}{2}\right)\Delta\epsilon_{x'x'}\right]^2. \end{aligned}\tag{C5}$$

Fits to the linear $(\frac{\Delta\rho}{\rho_0})_{A_{1g}}$ response vs $\frac{1-\nu_P}{2}\epsilon^{\text{meas}}_{x'x'}$ ($\epsilon^{\text{meas}}_{A_{1g}}$) incorrectly identify the slope, the effective measured $m^{A_{1g}}_{A_{1g}}$, as $m^{A_{1g}}_{A_{1g}} + \frac{(1+\nu_P)^2}{1-\nu_P}m^{B_{2g},B_{2g}}_{A_{1g}}\Delta\epsilon_{x'x'} = m^{A_{1g}}_{A_{1g}} + 2(\frac{1+\nu_P}{1-\nu_P})m^{B_{2g},B_{2g}}_{A_{1g}}\Delta\epsilon_{B_{2g}}$, so to accurately measure this quantity the neutral B_{2g} strain point must be correctly identified. If a similar procedure is followed for a sample experiencing A_{1g} and B_{1g} symmetry strain there is no error introduced to the measured $m^{A_{1g}}_{A_{1g}}$ for misidentification of the neutral strain point or for offsets between the B_{1g} and A_{1g} neutral points since there is no contribution from the quadratic response. Thus

estimates of $m^{A_{1g}}_{A_{1g}}$ extracted from samples that experience A_{1g} and B_{1g} symmetry strains are robust. Fits to the quadratic $(\frac{\Delta\rho}{\rho_0})_{A_{1g}}$ response vs $[\frac{1+\nu_P}{2}\epsilon^{\text{meas}}_{x'x'}]^2$ ($[\epsilon^{\text{meas}}_{B_{2g}}]^2$) correctly extract the quadratic coefficient $m^{B_{2g},B_{2g}}_{A_{1g}}$, independent of the neutral strain.

Two experimental observations confirm that we can correctly identify the neutral B_{2g} strain point. First, the estimates of $m^{A_{1g}}_{A_{1g}}$ [shown in Fig. 3(b) of the main text] are the same for crystals oriented such that they exhibit $A_{1g}+B_{2g}$ and $A_{1g}+B_{1g}$ strains. Second, misidentification of the B_{2g} neutral point would admix some amount of $m^{B_{2g},B_{2g}}_{A_{1g}}$ into the nominal measurement of $m^{A_{1g}}_{A_{1g}}$, which would introduce a strong temperature dependence—this is not observed.

APPENDIX D: FITTING $m^{B_{2g}}_{B_{2g}}$ AND $m^{B_{2g},B_{2g}}_{A_{1g}}$

The linear antisymmetric response to B_{2g} symmetry strain $m^{B_{2g}}_{B_{2g}}$ is extracted from a first order fit of $(\frac{\Delta\rho}{\rho_0})_{B_{2g}}$ versus $\epsilon_{B_{2g}}$. The temperature dependence of $m^{B_{2g}}_{B_{2g}}$ can then be fit to a Curie-Weiss functional form $m^{B_{2g}}_{B_{2g}}=\frac{\lambda}{a_0}(\frac{1}{T-\Theta})+m^{B_{2g}}_{B_{2g},0}$. The antisymmetric response deviates from a true Curie-Weiss behavior at high temperatures where the epoxy softens and at low temperatures due to the structural transition and disorder [4]. The optimal temperature range to extract the best Curie-Weiss fit is chosen following the procedure outline in Ref. [4], except that the reduced χ^2 error was minimized as opposed to the standard deviation. For the sample shown in the main text, the best fit temperature range was found to be 104–181 K. Extracted fit parameters are $\frac{\lambda}{a_0}=-2980\pm71$ K, $\Theta=75.8\pm0.6$ K, and $m^{B_{2g}}_{B_{2g},0}=17.3\pm0.7$, with $R^2_{\text{Adj}}=0.9995$.

The nonlinear symmetric response to antisymmetric B_{2g} strain $m^{B_{2g},B_{2g}}_{A_{1g}}$ was extracted from the quadratic coefficient of a second order fit of $(\frac{\Delta\rho}{\rho_0})_{A_{1g}}$ versus $\epsilon_{B_{2g}}$ using the same temperature range 104–181 K. As described in the main text, by symmetry the temperature dependence of $m^{B_{2g},B_{2g}}_{A_{1g}}$ is allowed to include the terms $\frac{a}{(T-\Theta)^2}+\frac{b}{T-\Theta}+c$. The Weiss temperature Θ is fixed to be 75.8 K from the Curie-Weiss fit of $m^{B_{2g}}_{B_{2g}}$. The fitted coefficients are $a=(2.0\pm0.2)\times10^7$ K^2, $b=(7.4\pm1)\times10^5$ K, and $c=(-6.7\pm0.9)\times10^3$, with $R^2_{\text{Adj}}=0.99655$. We can compare the magnitude of the contributions from individual terms in the fit. Close to the Weiss temperature (i.e., as $T-\Theta\to0$), we expect the quadratic term $(\frac{a}{(T-\Theta)^2})$ to dominate; however, at high temperatures the Curie-Weiss term $(\frac{b}{T-\Theta})$ is largest. The crossover point is roughly 23 K above the Weiss temperature, so for the accessible range of temperatures considered here (i.e., above $T_s=98$ K) the Curie-Weiss term is equal in magnitude or larger than the $\frac{a}{(T-\Theta)^2}$ component. It is not significantly larger over the whole temperature range and both terms are necessary to fully fit the response.

[1] J. W. Harter, Z. Y. Zhao, J.-Q. Yan, D. G. Mandrus, and D. Hsieh, Science **356**, 295 (2017).

[2] L. Zhao, C. A. Belvin, R. Liang, D. A. Bonn, W. N. Hardy, N. P. Armitage, and D. Hsieh, Nat. Phys. **13**, 250 (2017).

[3] M. Fiebig, V. V. Pavlov, and R. V. Pisarev, J. Opt. Soc. Am. B **22**, 96 (2005).

[4] H.-H. Kuo, J.-H. Chu, J. C. Palmstrom, S. A. Kivelson, and I. R. Fisher, Science **352**, 958 (2016).

[5] A. E. Böhmer and C. Meingast, C. R. Phys. **17**, 90 (2016).

[6] M. Yoshizawa, D. Kimura, T. Chiba, S. Simayi, Y. Nakanishi, K. Kihou, C.-H. Lee, A. Iyo, H. Eisaki, M. Nakajima, and S. Uchida, J. Phys. Soc. Jpn. **81**, 024604 (2012).

[7] A. E. Böhmer, P. Burger, F. Hardy, T. Wolf, P. Schweiss, R. Fromknecht, M. Reinecker, W. Schranz, and C. Meingast, Phys. Rev. Lett. **112**, 047001 (2014).

[8] Y. Gallais, R. M. Fernandes, I. Paul, L. Chauvière, Y.-X. Yang, M.-A. Méasson, M. Cazayous, A. Sacuto, D. Colson, and A. Forget, Phys. Rev. Lett. **111**, 267001 (2013).

[9] F. Kretzschmar, T. Böhm, U. Karahasanović, B. Muschler, A. Baum, D. Jost, J. Schmalian, S. Caprara, M. Grilli, C. Di Castro, J. G. Analytis, J.-H. Chu, I. R. Fisher, and R. Hackl, Nat. Phys. **12**, 560 (2016).

[10] J.-H. Chu, H.-H. Kuo, J. G. Analytis, and I. R. Fisher, Science **337**, 710 (2012).

[11] H.-H. Kuo and I. R. Fisher, Phys. Rev. Lett. **112**, 227001 (2014).

[12] H.-H. Kuo, M. C. Shapiro, S. C. Riggs, and I. R. Fisher, Phys. Rev. B **88**, 085113 (2013).

[13] For data shown in this paper, the expansion is done with respect to zero anisotropic strain $\Delta\rho=\rho(\epsilon)-\rho(\epsilon_{B_{1g/2g}}=0)$. For more details see Appendix C and Ref. [14].

[14] M. C. Shapiro, P. Hlobil, A. T. Hristov, A. V. Maharaj, and I. R. Fisher, Phys. Rev. B **92**, 235147 (2015).

[15] A standard delineation for the two A_{1g} symmetry terms in ϵ and $\Delta\rho/\rho_0$, which we also adopt here, is to separate in-plane [$\alpha=A_{1g,1}$ (i.e., x^2+y^2)] and out-of-plane responses [$\alpha=A_{1g,2}$ (i.e., z^2)].

[16] The irreducible representation notation can be related to the Cartesian and Voigt notations that have been used previously: $m^{B_{1g}}_{B_{1g}}=m_{xx,xx}-m_{xx,yy}=m_{11}-m_{12}$ and $m^{B_{2g}}_{B_{2g}}=2m_{xy,xy}=2m_{66}$.

[17] For the D_{4h} point symmetry, there are four independent combinations of terms in the fourth rank elastoresistivity tensor that can contribute to an A_{1g} symmetry elastoresistance response. Two possible linear combinations of strain that transform like an A_{1g} object are $\epsilon_{A_{1g,1}}=\frac{1}{2}[\epsilon_{x'x'}+\epsilon_{y'y'}]$ and $\epsilon_{A_{1g,2}}=\epsilon_{z'z'}$ and similarly for $\Delta\rho/\rho_0$; $\rho_{A_{1g,1}}=\frac{1}{2}[(\Delta\rho/\rho_0)_{x'x'}+(\Delta\rho/\rho_0)_{y'y'}]$ and $\rho_{A_{1g,2}}=(\Delta\rho/\rho_0)_{z'z'}$ [14]. For the measurements described in this paper, the effective out of plane Poisson ratio ν_z of the sample bonded to the PZT stack determines the strain in the z direction ($\epsilon_{zz}=-\nu_z\epsilon_{xx}$), which in turn affects the degree to which these combinations of coefficients admix in the measured symmetric response. Hence,

$$\left(\frac{\Delta\rho}{\rho_0}\right)_{A_{1g,1}}=m^{A_{1g,1}}_{A_{1g,1}}\epsilon_{A_{1g,1}}+m^{A_{1g,2}}_{A_{1g,1}}\epsilon_{A_{1g,2}}. \quad (4)$$

Since $\epsilon_{z'z'} = -\nu_z \epsilon_{x'x'}$ and $\epsilon_{y'y'} = -\nu_P \epsilon_{x'x'}$, we obtain

$$\left(\frac{\Delta\rho}{\rho_0}\right)_{A_{1g,1}} = \left(m^{A_{1g,1}}_{A_{1g,1}} - \frac{2\nu_z}{1-\nu_P} m^{A_{1g,2}}_{A_{1g,1}}\right)\epsilon_{A_{1g,1}} = m^{A_{1g}}_{A_{1g}} \epsilon_{A_{1g,1}} \quad (5)$$

defining the quantity $m^{A_{1g}}_{A_{1g}}$ used in the main text.

[18] J. H. Chu, J. G. Analytis, C. Kucharczyk, and I. R. Fisher, Phys. Rev. B **79**, 014506 (2009).

[19] While domain wall scattering can also contribute to the average resistivity of twinned samples in this regime, the linear temperature dependence implies that the dominant effect derives from the intrinsic increase in the average resistivity.

[20] C. A. M. dos Santos, A. de Campos, M. S. da Luz, B. D. White, J. J. Neumeier, B. S. de Lima, and C. Y. Shigue, J. Appl. Phys. **110**, 083703 (2011).